Alumina-Filled Polystyrene Micro- and Nanocomposites Prepared by Melt Mixing with and Without Latex Precompounding: Structure and Properties

S. Siengchin,[1] J. Karger-Kocsis,[1] R. Thomann[2]

[1]*Institute for Composite Materials (Institut für Verbundwerkstoffe GmbH), Kaiserslautern University of Technology, Erwin Schrödinger Str., D-67663 Kaiserslautern, Germany*
[2]*Institut für Makromolekulare Chemie und Freiburger Materialforschungszentrum, Albert-Ludwigs-Universität Freiburg, Stefan-Meier-Str. 31, D-79104 Freiburg, Germany*

Received 2 December 2006; accepted 4 March 2007
DOI 10.1002/app.26505
Published online 16 May 2007 in Wiley InterScience (www.interscience.wiley.com).

ABSTRACT: Alumina fillers were incorporated in polystyrene (PS) in 4.5 wt % by melt blending with and without latex precompounding. Latex precompounding was used for the latex-mediated predispersion of the alumina particles. The related masterbatch was produced by mixing PS latex with water dispersible boehmite alumina in various particle sizes followed by drying. The dispersion of the alumina in the PS was studied by transmission and scanning electron microscopy (TEM and SEM, respectively). The mechanical and thermomechanical properties of the PS composites were determined in uniaxial tensile, dynamic-mechanical thermal analysis (DMTA), and short-time creep tests performed at various temperatures. In addition, the melt flow of the composites was characterized in a plate/plate rheometer. It was found that direct melt mixing of the alumina with PS resulted in micro-, whereas the masterbatch technique in nanocomposites. The stiffness and resistance to creep (summarized in master curves) of the nanocomposites were improved compared to those of the microcomposites. The properties of the composites were upgraded by decreasing nominal size of the water dispersible alumina. The preparation technique and the size of the alumina particles affected the tensile strength, melt viscosity, and heat distortion temperature in lesser extent than the stiffness and thus compliance data. © 2007 Wiley Periodicals, Inc. J Appl Polym Sci 105: 2963–2972, 2007

Key words: polystyrene; nanocomposite; creep; structure-property relations; thermal properties; stiffness

INTRODUCTION

Nowadays, great effects are undertaken to improve the mechanical, thermal, and other properties (e.g., flame resistance, barrier properties, electric conductivity) of polymers using fillers of various shape factors, which may be dispersed on nanoscale in the resulting composites. For the modification of polystyrene (PS), for example, metal oxides,[1,2] organophilic modified layered silicates,[3–14] and single and multiwall carbon nanotubes[15–17] were already tried. It was recognized earlier that the preparation technique of the nanocomposites has a strong impact on the dispersion of the nanoparticles. One differentiates usually between *in situ* polymerization, melt blending, and solution/dispersion preparation techniques.[18] The latter grouping also covers the latex compounding/latex coagulation methods. Major benefits of the ''latex route'' are listed below. It is noteworthy that for the production of rubber nanocomposites, the latex coagulation is already widely used.[19–22] Many polymers are produced by suspension and emulsion polymerizations in aqueous media. The related suspension, emulsions, or latices (for rubbers) can be easy modified with water swellable or water dispersible particles. Water swellable are for example several layered silicates (montmorillonites, bentonites) bearing intergallery Na^+ ions. Via hydration of the intergallery cations intercalated and exfoliated structures can be achieved. Among the water dispersible commercially available nanofillers, alumina should be mentioned. To produce nanocomposites using aqueous dispersions, slurries are not only an affordable method (no organophilic modification is needed for the fillers) but are also associated with reduced health hazard. Recall that the particles introduced are in micron range and become nanoscaled only in the aqueous media. In the follow-up steps (coagulation, drying etc.), the nanoparticles are embedded in the polymer, which guarantees easy handling and minimized health risk. Apart from rubbers,[19–22] this ''latex-route'' is followed for various polymers, including PS,[23–28] to produce various nanocomposites. There is a further scientific beauty with this approach: it is possible to produce micro- and nanocomposites using

Correspondence to: J. Karger-Kocsis (karger@ivw.uni-kl.de).

Journal of Applied Polymer Science, Vol. 105, 2963–2972 (2007)

the same components (e.g. Ref. 28). This is very straightforward to figure out whether a ''nanoeffect'' exists and what is its influence on the material performance.

Water dispersible alumina, offered by the company Sasol, were already incorporated in thermoplastics,[29–31] thermosets,[32] and even in thermoplastic rubbers,[33] however, usually after their organophilic modification. In pristine form, alumina nanoparticles were dispersed in polyurethane rubber through latex compounding.[34] Note that the alumina particles remain in aggregates (micron-sized) when introduced in polymers by melt blending.

The aim of this work was to produce PS/alumina micro- and nanocomposites and to study their properties. A further aim of this work was to check the effect of the mean particle size of the water dispersible alumina. Microcomposites were produced by direct melt blending (incorporation of the alumina powder in the PS melt during kneading), whereas nanocomposites by a combined method. In the latter case, the alumina particles were dispersed in an aqueous PS latex prior to its drying and incorporation in the PS by melt blending (referred to masterbatch technique).

EXPERIMENTAL

Materials and preparation of composites

Two types of water disperable boehmite alumina (Disperal® P2 and Dispal®11N7-80 of Sasol GmbH, Hamburg, Germany) served as fillers. Their specifications are listed in Table I. PS latex with 50 wt % dry content (Baystal SX 1160) was supplied by Polymer Latex GmbH (Marl, Germany). Granulated PS (Polystyrol 158 K Glasklar, BASF, Ludwigshafen, Germany) was utilized as polymeric matrix for all composite systems. Its volumetric melt flow rate (MVR at 200°C/5 kg) was 3 cm^3/10 min.

The PS/alumina nanocomposites were prepared by two methods: (a) direct melt compounding and (b) melt compounding using a masterbatch produced from PS latex containing alumina particle (masterbatch technique). The molecular characteristics of the PSs in latex and granulate forms were not determined; however, they were similar according to suppliers' information. The alumina content in the corresponding composites was set for 4.5 wt %. Melt mixing occurred in laboratory kneader (Type 50 of Brabender, Duisburg, Germany) at T = 180°C and rotor speed of 60 rpm. The alumina powder (direct method) or alumina-containing PS masterbatch (masterbatch technique) was introduced after melt mastication (granulates + dried latex) for 2 min. The duration of the melt mixing for both direct and masterbatch techniques was 6 min.

TABLE I
Specification of the Water Dispersible Boehmite Aluminas as Delivered by Sasol Germany GmbH

Characteristics/Type	Disperal® P2	Dispal® 11N7-80
Al_2O_3 (%)	72	80
Na_2O (%)	0.002	0.002
NO_3 (%)	4.0	0.1
Loose bulk density (g/L)	850	620
Specific surface area (m^2/g)	260	100
Mean powder particle size (μm)	45	40
Mean dispersed particle size in water (nm)	25	220

The masterbatch was produced as follows. First, an aqueous alumina slurry (10 wt %) was prepared at ambient temperature through mechanical stirring for 30 min. Then, the PS latex was introduced in this slurry and stirred for further 30 min. The resulting slurry was poured in a framed glass plate and dried for 48 h at room temperature (RT) and for 12 h at 60°C. Note that this condition does not produce a void-free film from PS latex as the glass transition temperature (T_g) of PS is much higher than RT. However, a void-free film was no prerequsite owing to the subsequent melt mixing process. For reference purpose, a PS containing 25 wt % PS from the latex was selected. This composition considers the latex-derived PS content of the composites.

The compounds after melt mixing in the Brabender kneader were compression molded in 1-mm thick sheets at T = 180°C using a hot press (EP-Stanzteil, Wallenhorst, Germany).

Characterization of the alumina dispersion

The dispersion of alumina in the PS micro- and nanocomposites was assessed by transmission and scanning electron microscopy (TEM and SEM, respectively). TEM measurements were carried out with a Zeiss LEO 912 Omega transmission electron microscopic (Oberkochen, Germany), applying an acceleration voltage of 120 keV. Thin sections (~ 50 nm) were cut at RT with a Diatome diamond knife using an Ultracut E microtome (Reichert and Jung, Vienna, Austria). The dispersion state of the alumina particles was studied by SEM, too. Here, the fracture surfaces of the tensile loaded specimens were subjected to SEM inspection in a JSM 5400 device of Jeol (Tokyo, Japan). The surfaces were gold coated prior to SEM performed at 25 kV acceleration voltage.

Testing

Dynamic-mechanical thermal analysis (DMTA) was made in single cantilever mode at 0.1–10 Hz frequen-

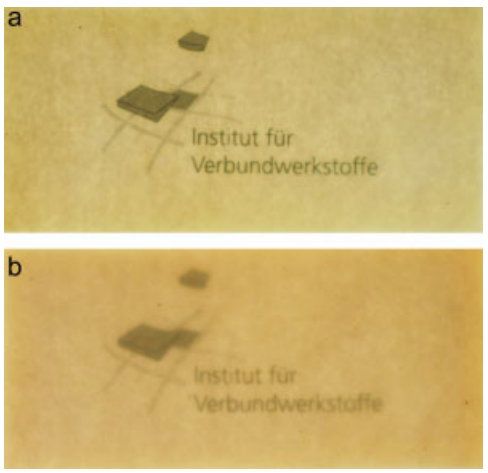

Figure 1 Macrophotographs showing the difference in the transparency between PS/P2 composites at the same thickness (=1.1 mm) produced by the masterbatch technique (a) and direct melt compounding (b). [Color figure can be viewed in the online issue, which is available at www.interscience.wiley.com.]

cies using a Q800 apparatus (TA Instruments, New Castle). The storage modulus (E') along with mechanical loss factor (tan δ) was determined as a function of the temperature ($T = -50°C \ldots +130°C$). The strain applied was 0.01%. Tests were run in the above temperature and frequency ranges by increasing the temperature stepwise by 3°C and equilibrating the specimen at each temperature for 5 min prior to start with the frequency sweep (set for 0.1, 1, and 10 Hz, respectively). The sample dimensions were 10 × 35 × 3 mm^3 (width × length × thickness).

Short-time creep tests were made in tensile mode at different temperatures using the above DMA apparatus. The creep and recoverable compliance were determined as a function of the time (t_{creep} = 30 min and $t_{recovery}$ = 120 min). The tensile stress applied was 4 MPa (at 0.5% strain). This was derived from a test series checking the presence of linear isochronous deformation. The specimens' dimensions were 9 × 35 × 0.4 mm^3 (width × length × thickness).

To get a clearer picture on the creep response of the PS/alumina composites, the time-temperature superposition principle was adopted for short-term creep tests performed at various temperatures. The tensile stress applied here was 3 MPa. The temperature dependence of the creep response of the PS and its composites was studied in the range from 20 to 75°C. In this temperature range, isothermal tests were run on the same specimen by increasing the temperature stepwise by 5°C. Prior to the creep measurement (duration 15 min), the specimen was equilibrated for 5 min at each temperature.

The heat distortion temperature (HDT) was determined in three point bending mode using the same DMTA device. The stress applied was 0.46 MPa and the heating rate was set for 2°C/min (similar to ASTM D 648). The sample dimensions were 60 × 12 × 3 mm^3 (width × length × thickness).

In addition, tensile tests were performed on dumbbell-shaped specimens (S3A type according to DIN 53504) on a Zwick 1474 universal testing machine (Ulm, Germany). Tests were run at RT with v = 2 mm/min crosshead speed and the related modulus, strength and elongation at break values were determined.

A controlled strain rheometer (ARES of Rheometric Scientific, NJ, USA) was utilized in parallel plate configuration (diameter of the plate: 25 mm) to measure the melt rheology of the PS and its composites at T = 180°C. Oscillatory shear measurements were performed on each sample by setting the strain amplitude for 1%. This was derived from a strain sweep test series checking the presence of the linear viscoelastic region. The gap between the plates was 2 mm.

RESULTS AND DISCUSSION

Alumina dispersion

The composite sheets produced by the masterbatch technique were more translucent at the same thickness than those prepared by direct melt blending (Figure 1). This is the first hint for the difference in the dispersion stage of the alumina particles in the corresponding composites.

TEM pictures taken from the direct melt compounded PS composites evidence the presence of large, microscale aggregates of the alumina particles. They are thus correctly referred to microcomposites. The only difference between P2 and 11N7-80 particles is that the latter is also dispersed in smaller aggregates in the PS matrix [cf. Fig. 2(b)] by contrast to P2 [cf. Fig. 2(a)]. Characteristic TEM pictures taken from the composites produced by the masterbatch technique in Figure 3 show that the alumina particles are nanoscaled dispersed in them. One can also recognize

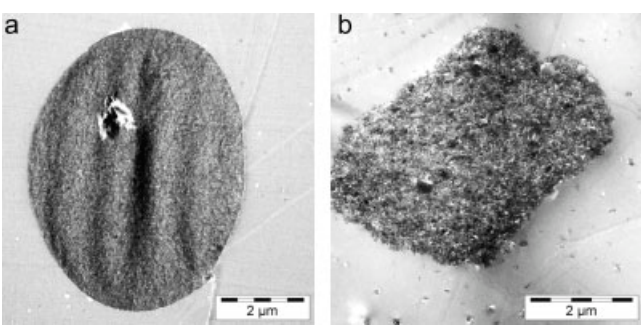

Figure 2 TEM pictures from the PS/alumina microcomposites produced by melt blending with P2 (a) and 11N7-80 (b) alumina, respectively.

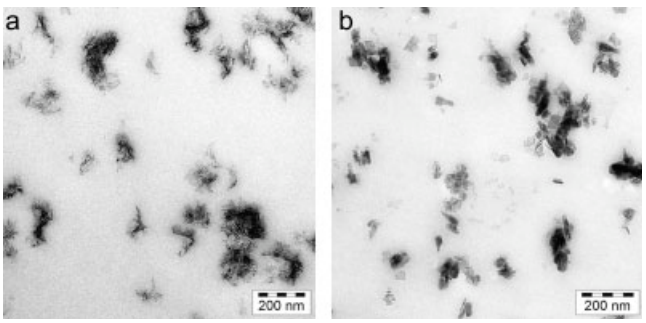

Figure 3 TEM pictures from the PS/alumina nanocomposites produced by masterbatch technique with P2 (a) and 11N7-80 (b) alumina, respectively.

that the size of the primary particles is much smaller for P2 than for 11N7-80, which is in harmony with the data in Table I. On the other hand, the particles are still aggregated in the related nanocomposites (cf. Fig. 3).

The reason for this aggregation is due to the PS latex mediated dispersion of the alumina in the PS. By reducing the compounding temperature when combining the PS with the dried PS/alumina from the latex (masterbatch) it could be shown that the alumina particles are located in the boundary layer between the PS latex particles (cf. Fig. 4). This finding is in analogy with results reported on pristine clay modified natural rubber lattices.[19,22] The alumina particles become further dispersed mostly owing to shear forces in the fused PS during compounding.

SEM pictures taken from the fracture surfaces of tensile loaded specimens give further insight in the alumina dispersion. This is due to the larger viewfield in SEM compared to TEM. Figure 5 compares the fracture surfaces of the PS/P2 composites produced differently. Secondary cracking due to the large particles causing microductile deformation of the PS is obvious for the microcomposites [cf. Fig. 5(a)]. The onset of secondary cracking, manifesting in a characteristic dimple pattern, suggests that the alumina particles in the nanocomposite are homogeneously dispersed [cf. Fig. 5(b)]. The same statement holds for the PS composites with coarse alumina particles (cf. Fig. 6). By comparing Figures 5(a) and 6(a) one may conclude that the 11N7-80 particles are better dispersed through direct melt blending in the PS matrix than the P2 particles.

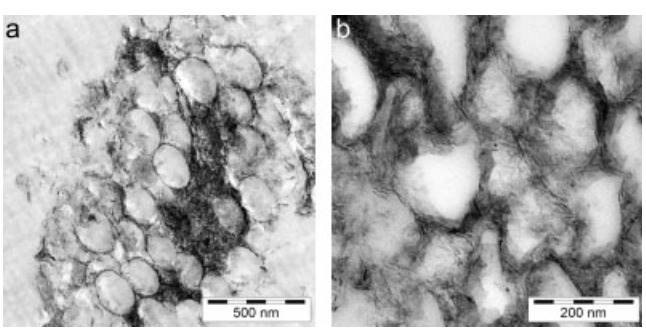

Figure 4 TEM pictures taken from the PS/P2 nanocomposites produced by the masterbatch technique by setting the temperature of the compounding for $T = 165°C$.

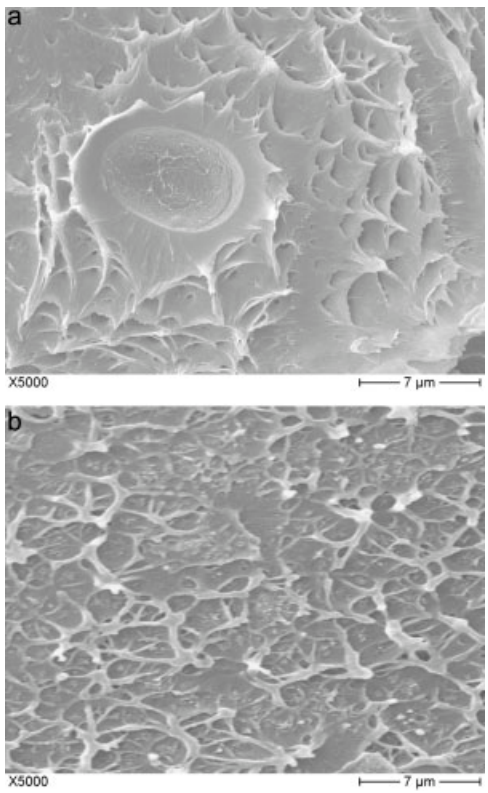

Figure 5 SEM pictures from the fracture surfaces of the PS/P2 composites produced by direct blending (a) and masterbatch technique (b), respectively.

Properties

DMTA response

Figure 7 depicts the storage modulus (E′) and mechanical loss factor (tan δ) as a function of temperature for the composites containing 4.5 wt % of alumina particles produced by various methods. Note that incorporation of alumina particles in PS resulted in a pronounced stiffness enhancement below the T_g. This reinforcing effect was accompanied with a shift in the T_g towards higher temperature. This can be assigned to the formation of an interphase with reduced molecular mobility. It is very surprising that the intensity of the T_g relaxation increases by adding alumina as usually the opposite trend occurs. This may be linked with some constraint effects in the composites for which the authors have no explanation. Figure 7 also shows that the stiffness of the com-

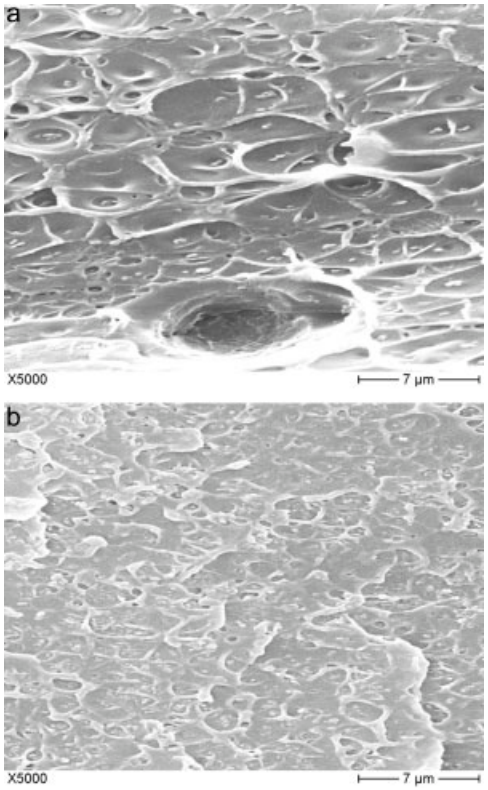

Figure 6 SEM pictures from the fracture surfaces of the PS/11N7-80 composites produced by direct blending (a) and masterbatch technique (b), respectively.

posite is governed by their production (yielding micro- and nanocomposites, respectively) and practically not influenced by the primary particle size of the alumina. Recall that under primary particle size that one achievable in water slurry is meant (cf. Table I).

The stiffness of PS/alumina composites which were prepared by direct compounding was always inferior to those produced by the masterbatch technique. An attempt was made to apply the time-temperature superposition principle to the DMTA data measured in function of both temperature (T = −50°C … +130°C) and frequency (f = 0.1–10 Hz). Master curves in form of E′ versus frequency were produced by superimoposing the storage modulus versus frequency traces using the time-temperature superposition principle. A reference temperature (T_0 = 70°C) was used for this superposition process. Note that the related shift factor (a_T) is given:

$$a_T = \frac{E'(T)}{E'(T_0)} \tag{1}$$

The shift factors are linked with temperature via the Williams-Landel-Ferry (WLF) equation (e.g., Refs. 35 and 36), as follows:

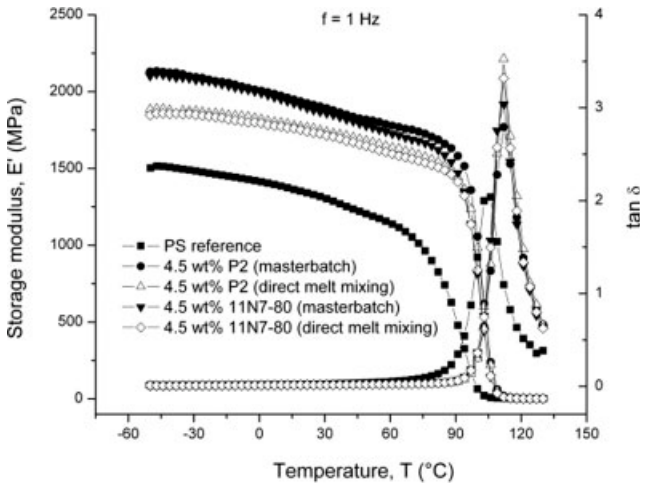

Figure 7 E' versus T and tan δ versus T traces for the PS/alumina composites produced by various methods. Designations: ■ – PS reference; ● – masterbatch technique; P2-content 4.5 wt %; △ – direct melt mixing; P2-content 4.5 wt %; ▼ – masterbatch technique; 11N7-80-content 4.5 wt %; ◇ – direct melt mixing; 11N7-80-content 4.5 wt %.

$$\log(a_T) = \log\left(\frac{f}{f_0}\right) = \frac{-C_1(T - T_0)}{C_2 + (T - T_0)} \tag{2}$$

where C_1 and C_2 are constants and T_0 is the reference temperature (=70°C).

The traces in Figure 8 indicate again that the effect of the preparation method (and alumina dispersion) is more pronounced than that of primary particle size of the alumina used.

Figure 9 displays the course of the experimentally determined a_T values as a function of the temperature. The temperature range selected agrees with that of the creep tests. One can recognize that the experimental a_T data follow the WLF prediction albeit the latter strictly holds for polymers above their T_g. From the temperature dependence of the shift factor the

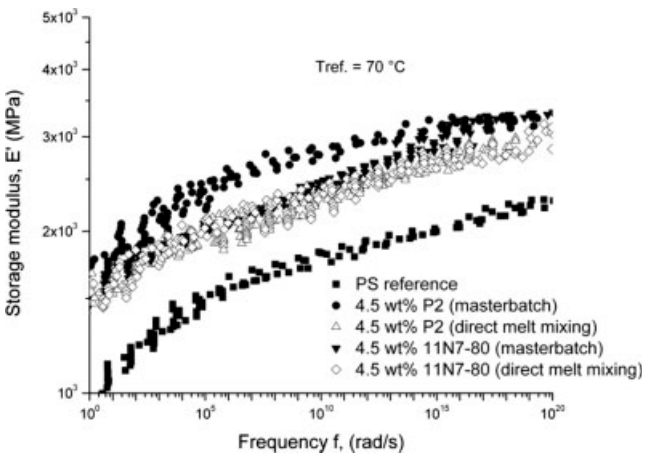

Figure 8 E' versus frequency traces for the PS/alumina composites at $T_{ref.}$ = 70°C. For designations, cf. Figure 7.

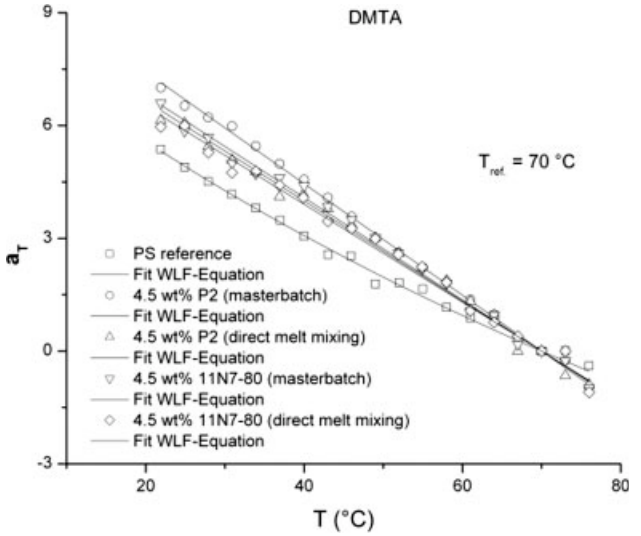

Figure 9 Experimental shift factors along with the related WLF fits in the temperature range T = 20–75°C for the systems studied.

activation energy (ΔH) can be computed by the following equation:

$$\ln a_T = \frac{\Delta H}{R}\left(\frac{1}{T} - \frac{1}{T_0}\right) \quad (3)$$

where R is the universal gas constant. On the basis of the experimental data in Figure 9, the following ΔH values were derived: PS reference = 214 kJ/mol; PS + 4.5 wt % P2 – direct and masterbatch techniques, respectively: 267 and 281 kJ/mol; PS + 4.5 wt % 11N7-80 – direct and masterbatch techniques, respectively: 263 and 271 kJ/mol. The increase in ΔH with alumina filling suggests that the mobility of the PS chains was reduced in both PS micro- and nanocomposites. This is in concert with the observed shift in the corresponding tan δ versus T traces (cf. Fig. 7). Moreover, the change in the ΔH values show the difference between micro- (lower ΔH) and nanocompsites (higher ΔH), and even the difference in the dispersion stage of the nanocomposites (ΔH is higher for the PS/P2 than for the PS/11N7-80 nanocomposite).

Creep behavior

Figures 10 and 11 display the creep and recovered compliance values for the PS and its alumina composites produced by direct melt mixing and masterbatch methods. The addition of alumina particles into PS matrix resulted in a considerable reduction in the creep compliance, as shown by the plots of creep and recovered compliances against time. The decrease in creep compliance is due to the reinforcing effect of the alumina particles. For the composites containing 4.5 wt % P2 for example the creep compliance was

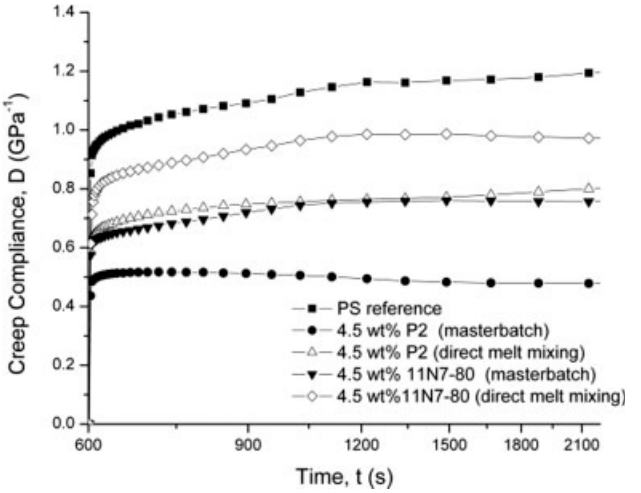

Figure 10 Creep of the reference PS and its alumina composites prepared by different methods at RT (Note: stress applied at t = 10 min). Designations: ■ – PS reference; ● – masterbatch technique; P2-content 4.5 wt %; △ – direct melt mixing; P2-content 4.5 wt %; ▼ – masterbatch technique; 11N7-80-content 4.5 wt %; ◇ – direct melt mixing; 11N7-80-content 4.5 wt %.

reduced by ~ 55 and 30% compared the reference PS when produced by the masterbatch technique and direct melt compounding, respectively. The most striking finding is that the primary particle size of the alumina likely affects the creep behavior. Note that the resistance to creep increases with decreasing alumina particle size.

Figure 12 demonstrates the effect of increasing temperature on the creep compliance of the PS and its nanocomposite with 11N7-80 alumina. Note that the creep compliance increases with increasing temperature. On the other hand, one can recognize that the

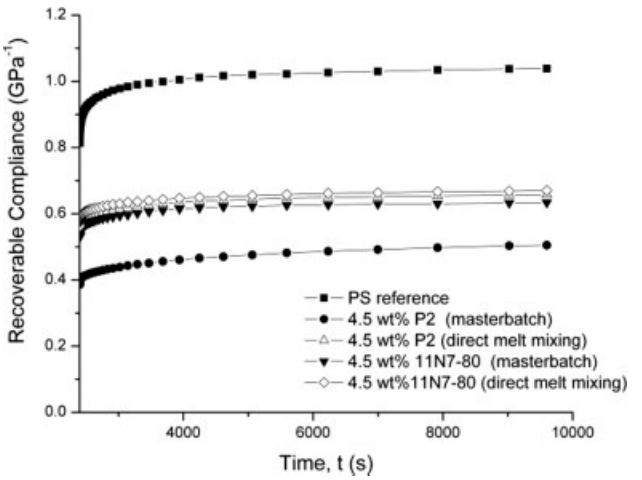

Figure 11 Creep recovery of the reference PS and its alumina composites prepared by different methods at RT (Note: stress removal at t = 40 min). For designations, cf. Figure 10.

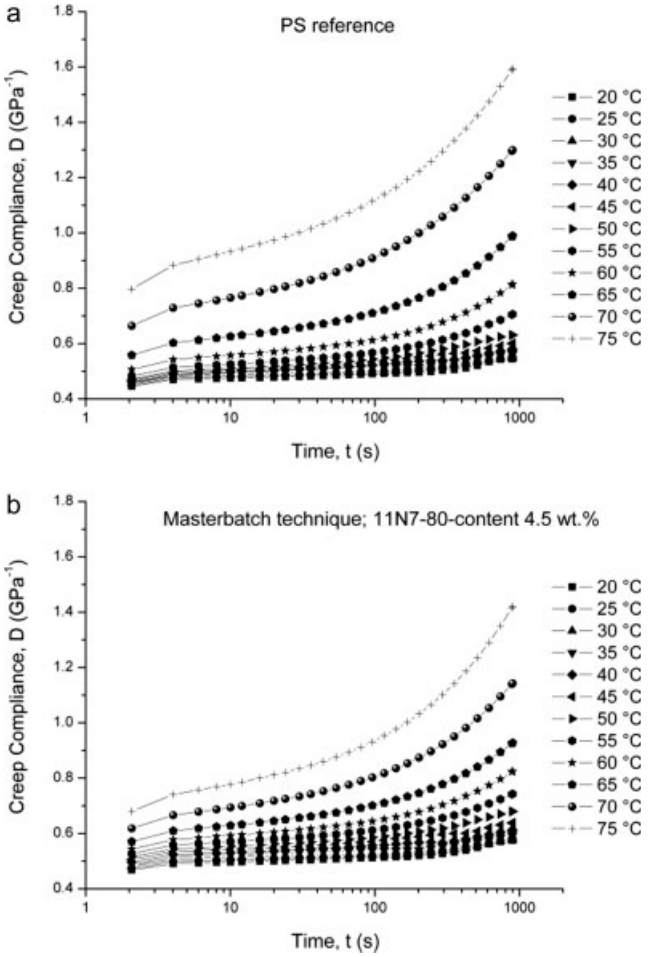

Figure 12 Effect of temperature on the tensile creep of PS (a) and its composite with 4.5 wt % alumina 11N7-80 prepared by the masterbatch technique (b).

creep compliance decreased markedly for the PS/11N7-80 nanocomposite, especially at higher temperatures [cf. Fig. 12(a,b)].

Creep master curves were constructed by time-temperature superposition principle: The creep at a given temperature (T_1) is related to the creep at another temperature (T_2) by considering the shift factor (a_T) along the time scale (t):[35,36]

$$D(t, T_1) = \frac{D(t, T_2)}{a_T} \tag{4}$$

where D is the creep compliance at the time t.

The shift factors can be also correlated with temperature using the WLF equation [cf. eq. (2)]. To highlight the differences $T = 70°C$ was taken as reference temperature. The corresponding master curves are summarized in Figure 13. The reinforcing effect of the alumina particles is obvious in this figure.

As, expected according to Figures 10 and 11, the primary particle size, or more exactly the dispersion state of the alumina, are well reflected in the creep

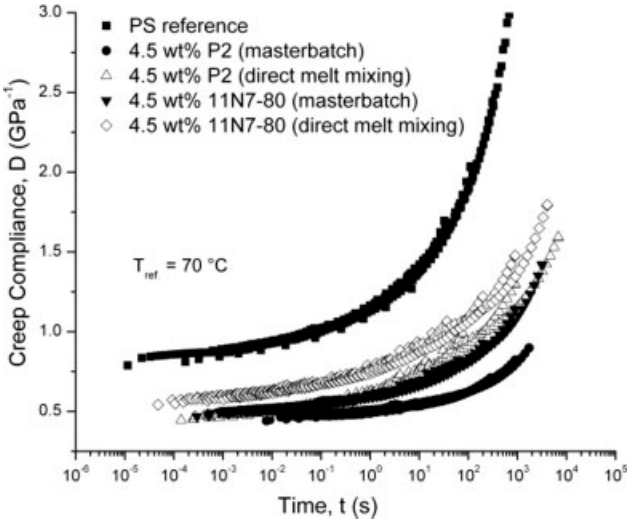

Figure 13 Creep master curves (compliance versus time constructed by considering $T_{ref.} = 70°C$ for the PS reference and its micro- (direct melt blended) and nanocomposites (produced by the masterbatch technique).

master curves (cf. Fig. 13). The change from micro- to nanocomposite reduces further the creep compliance. This may be associated with pronounced changes in the creep rate. It was recently reported that the creep rate is hardly affected by the dispersion state of layered silicates.[37] This claim holds for the PS/11N7-80 composites and also for the direct melt blended PS/P2, at least in a given time interval (cf. initial parallel run of the creep curves in Fig. 13). On the other hand, the PS/P2 nanocomposite exhibits a creep rate differing substantially from that of the PS matrix. It has to be clarified next that this behavior is due to the dispersion of P2 (that has to be characterized more

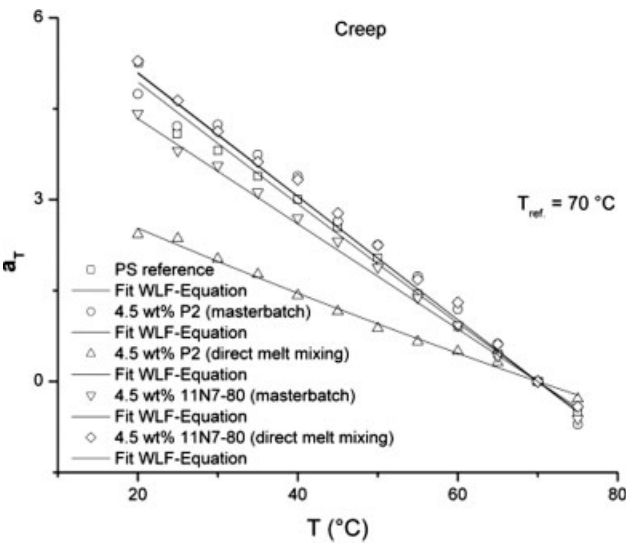

Figure 14 Experimental shift factors along with the related WLF fits in the creep temperature range $T = 20$–$75°C$ for the systems studied.

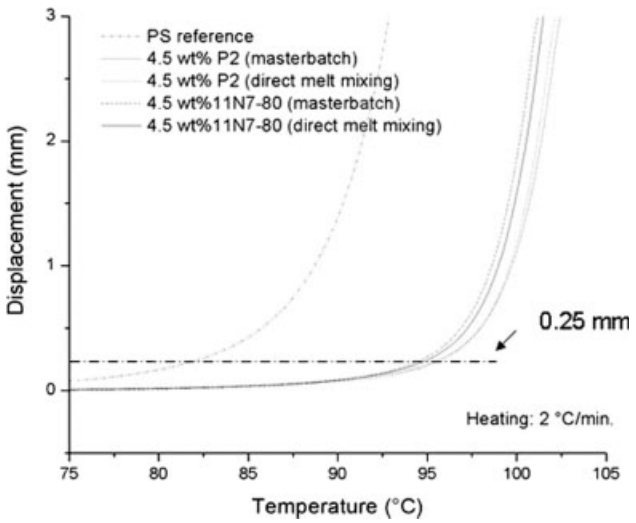

Figure 15 Displacement versus temperature for the PS/alumina composites produced by various methods.

detailed), or to other reasons (material inhomogeneity, selection of the reference temperature). It has to be mentioned that such creep behavior was already reported for thermoplastic nanocomposites, however, with a semicrystalline matrix.[38]

Figure 14 depicts the experimentally determined a_T values for the studied creep interval. One can see that the experimental a_T data obey the WLF equation, similar to the DMTA results (cf. Fig. 9). Equation (3) was adopted to compute the creep activation energy values. They were found as given below: PS reference = 196 kJ/mol; PS + 4.5 wt % P2 – direct and masterbatch techniques, respectively: 99 and 198 kJ/mol; PS + 4.5 wt % 11N7-80 – direct and masterbatch techniques, respectively: 204 and 172 kJ/mol. Comparing these activation energies with those from the DMTA (listed above) a fair agreement can only be noticed for the neat PS. The large discrepancy for the alumina filled micro- and nanocomposites suggests that the creep response is far more sensitive to the dispersion stage of the filler in the related specimens than in the DMTA test - although both tests were performed in the linear viscoelastic range. However, the loading configuration (single cantilever versus uniaxial tensile) and especially the related strain values (0.01 vs. 0.38% per corresponding to the stress applied, viz. 0.13 versus 3 MPa/for the DMTA and creep tests, respectively) differed considerably from one another. This finding means that numerous parallel tests are required to determine reliable creep master curves.

HDT

The HDT is given by that temperature at which the specimen deflection reaches 0.25 mm under a given flexural load (in this case 0.46 MPa). According to the related standard (ASTM D 648), the heating rate is 2°C/min. Recall that during our measurements in air the heating rate was 2°C/min. In principle, the HDT value represents a point in the flexural creep response when the displacement is plotted against the temperature. Figure 15 shows the related traces. One can see that the HDT values of the composites (94–95°C) are far beyond that of the reference PS (82°C). On the other hand, the effects of composite preparation and primary particle size of the alumina are marginal (cf. Table II).

Tensile tests

Results of the tensile mechanical tests are given in Table II. One can notice that the stiffness of the composites is strongly enhanced by adding alumina. The preparation techniques, yielding micro- and nanocomposites, have also a great impact on the stiffness. The latter is more than 20% higher for the nano- than for the microcomposites. The tensile strength is less sensitive for the composite preparation than the stiffness. Nevertheless, the strength of the composites was more than 40% higher than that of the reference PS (cf. Table II). Elongation at break values suggests that the improvement in the stiffness and strength was achieved at the cost of the ductility of the composites.

TABLE II
Tensile Mechanical Characteristics and HDT Data of the PS Reference and Alumina-Reinforced PS Composites Prepared by Various Methods

	Material				
		Masterbatch technique		Direct melt mixing	
Property	PS/dried PS latex 75/25 wt % (PS reference)	PS/4.5 wt % P2	PS/4.5 wt % 11N7-80	PS/4.5 wt % P2	PS/4.5 wt % 11N7-80
Tensile modulus (MPa)	3026 ± 268	4876 ± 159	4789 ± 196	3987 ± 162	3899 ± 206
Tensile strength (MPa)	27 ± 0.9	43 ± 1.3	40 ± 1.8	40 ± 1.8	39 ± 0.9
Elongation at break (%)	5.7 ± 0.9	1.1 ± 0.1	1.3 ± 0.02	0.8 ± 0.04	1.3 ± 0.07
HDT (°C)	82.3 ± 0.4	95.7 ± 0.5	94.3 ± 0.6	95.9 ± 0.4	94.9 ± 0.3

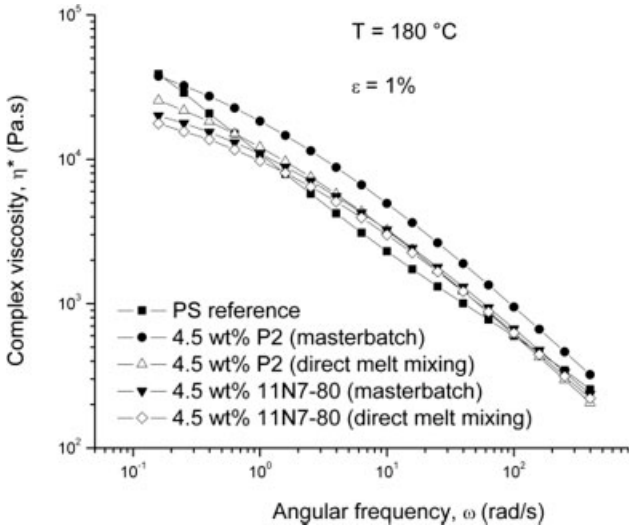

Figure 16 Viscosity versus angular frequency for the reference PS and its alumina composites prepared by different methods at $T = 180^{\circ}C$.

Melt rheology

The reference PS show clear shear thinning behavior in the viscosity versus angular frequency curves (cf. Fig. 16). Incorporation of the alumina micro- and nanoparticles is likely accompanied with the onset of a plateau at the low angular frequencies. This can be assigned to a solidlike stage owing to the reinforcing effect of the alumina. Note that the viscosity of the nanocomposites is always higher than that of the corresponding microcomposites albeit the difference is relatively small. Further investigation are however, needed to clarify whether a plateau viscosity exists and reflects the dispersion state of the alumina particles accordingly.

CONCLUSION

This work was aimed at comparing the mechanical, thermal, and rheological properties of PS/alumina composites in which the alumina particles are micro- and nanoscaled dispersed. The related dispersion was achieved by melt compounding with (masterbatch technique) and without (direct melt compounding) precompounding a PS latex with water-dispersible alumina of various primary particle sizes. The masterbatch technique resulted in nano-, whereas direct melt blending in PS/alumina microcomposites. This was demonstrated by TEM and SEM investigations. The stiffness, measured in DMTA and tensile tests, of the nanocomposites was markedly higher than that of the microcomposites. The tensile strength and HDT values were also enhanced, however, did not reflect the effects of composite preparation and alumina particle size. The creep results, especially when summarized in compliance versus time master curves, proved to be very sensitive indicates for both alumina size and dispersion type. Rheological tests at very low angular frequencies seem to be also a useful tool to detect effects of the alumina dispersion state.

S. Siengchin thank the DFG (German Science Foundation) for the fellowship in the framework of the graduate school GRK 814.

References

1. Wang, Z.; Li, G.; Peng, H.; Zhang, Z.; Wang, X. J Mater Sci 2005, 40, 6433.
2. Ma, C.-C. M.; Chen, Y.-J.; Kuan, H.-C. J Appl Polym Sci 2005, 98, 2266.
3. Sohn, J.-I.; Lee, C. H.; Lim, S. T.; Kim, T. H.; Choi, H. J.; Jhon, M. S. J Mater Sci 2003, 38, 1849.
4. Vuluga, Z.; Donescu, D.; Radovici, C.; Marinache, D.; Şerban, S.; Vuluga, D. M.; Paven, H. Mater Plast 2004, 41, 3.
5. Dazhu, C.; Haiyang, Y.; Pingsheng, H.; Weian, Z. Compos Sci Technol 2005, 65, 1593.
6. Jeong, H. M.; Choi, J. S.; Ahn, Y. T.; Kwon, K. H. J Appl Polym Sci 2006, 99, 2841.
7. Yilmazer, U.; Ozden, G. Polym Compos 2006, 27, 249.
8. Lim, Y. T.; Park, O. O. J. Macromol Rapid Commun 2000, 21, 231.
9. Hoffmann, B.; Dietrich, C.; Thomann, R.; Friedrich, C.; Mülhaupt, R. Macromol Rapid Commun 2000, 21, 57.
10. Meincke, O.; Hoffmann, B.; Dietrich, C.; Thomann, R.; Friedrich, C. Macromol Chem Phys 2003, 204, 823.
11. Sikka, M.; Cerini, L. N.; Ghosh, S. S.; Winey, K. I. J Polym Sci Part B: Polym Phys 1996, 34, 1443.
12. Kim, T. H.; Lim, S. T.; Lee, C. H.; Choi, H. J.; Jhon, M. S. J Appl Polym Sci 2003, 87, 2106.
13. Morgan, A. B.; Gilman, J. W. J Appl Polym Sci 2003, 87, 1329.
14. Beyer, F. L.; Tan, N. C. B.; Dasgupta, A.; Galvin, M. E. Chem Mater 2002, 14, 2983.
15. Loos, J.; Alexeev, A.; Grossiord, N.; Koning C. E.; Regev, O. Ultramicroscopy 2005, 104, 160.
16. Chang, T.-E.; Kisliuk, A.; Rhodes, S. M.; Brittain, W. J.; Sokolov, A. P. Polymer 2006, 47, 7740.
17. Wang, Z.; Lu, M.; Li, H.-L.; Guo, X.-Y. Mater Chem Phys 2006, 100, 77.
18. Karger-Kocsis, J.; Zhang, Z. In Mechanical Properties of Polymers Based on Nanostructure and Morphology; Michler, G. H., Baltá-Calleja, F. J., Eds.; CRC Press: Boca Raton, FL, 2005; Chapter 13, pp 553–602, .
19. Varghese, S.; Karger-Kocsis, J. In Polymer Composites from Nano- to Macro-Scale; Friedrich, K., Fakirov, S., Zhang, Z., Eds.; Springer: Berlin, 2005; Chapter 5, pp 77–90.
20. Karger-Kocsis, J.; Wu, C.-M. Polym Eng Sci 2004, 44, 1083.
21. Wu, J.-P.; Wang, Y.-Q.; Zhang, H.-F.; Wang, Y.-Z.; Yu, D.-S.; Zhang, L.-Q.; Yang, J. Compos Sci Technol 2005, 65, 1195.
22. Varghese, S.; Gatos, K. G.; Apostolov, A. A.; Karger-Kocsis, J. J Appl Polym Sci 2004, 92, 543.
23. Wang, C.; Wang, Q.; Chen, X. Macromol Mater Eng 2005, 290, 920.
24. Li, H.; Yu, Y.; Yang, Y. Eur Polym J 2005, 41, 2016.
25. Li, H.; You, B.; Gu, G.; Wu, L.; Chen, G. Polym Int 2005, 54, 191.
26. Uğur, S.; Alemdar, A.; Pekcan, Ö. Polym Compos 2006, 27, 299.
27. Ding, P.; Qu, B. J Appl Polym Sci 2006, 101, 3758.
28. Siengchin, S.; Karger-Kocsis, J.; Apostolov, A. A.; Thomann, R. J Appl Polym Sci, to appear.

29. Özdilek, C.; Kazimierczak, K.; van der Beek, D.; Picken, S. J. Polymer 2004, 45, 5207.
30. Sugama, T.; Gawlik, K. Polym Polym Compos 2004, 12, 153.
31. Xalter, R.; Halbach, T. S.; Mülhaupt, R. Macromol Symp 2006, 236, 145.
32. Shahid, N.; Villate, R. G.; Barron, A. R. Compos Sci Technol 2005, 65, 2250.
33. Adhikari, R.; Henning, S.; Lebek, W.; Godehardt, R.; Ilisch, S.; Michler, G. H. Macromol Symp 2006, 231, 116.
34. Gatos, K. G.; Alcázar, J. G. M.; Psarras, G. C.; Thomann, R.; Karger-Kocsis, J. Compos Sci Technol 2007, 67, 157.
35. Ferry, J. D. Viscoelastic Properties of Polymers, Wiley: New York, 1980.
36. Palade, L. I.; Verney, V.; Attane, P. Macromolecules 1995, 28, 7051.
37. Siengchin, S.; Karger-Kocsis, J. Macromol Rapid Commun 2006, 27, 2090.
38. Yang, J.-L.; Zhang, Z.; Schlarb, A. K.; Friedrich, K. Polymer 2006, 2791.